TWO APPROACHES TO MICROMACHINING SI HEAT EXCHANGER FOR JOULE-THOMSON CRYOSURGICAL PROBES

Weibin Zhu[1*], Michael J. White[2], Daniel W. Hoch[3], Gregory F. Nellis[2], Sanford A. Klein[2], Yogesh B. Gianchandani[1]
[1]*Department of Mechanical Engineering, University of Michigan, Ann Arbor, USA*
[2]*Department of Mechanical Engineering, University of Wisconsin, Madison, USA*
[3]*Department of Engineering Technology, University of North Carolina, Charlotte, USA*

ABSTRACT

This paper describes results from two types of micromachined recuperative heat exchangers intended for Joule-Thomson (J-T) cryosurgical probes, which require high stream-to-stream thermal conductance while restricting parasitic stream-wise (axial) conduction. In design A, rows of fins composed of high conductivity silicon are bonded onto a 100 μm thick base plate composed of low conductivity Pyrex glass. This planar device has a footprint of 6×1.5 cm^2 and 2.5 mm thickness, and is fabricated using a 5-mask process. In design B, numerous high-conductivity silicon plates alternating with low-conductivity Pyrex spacers are stacked together. This has a footprint of 1×1cm^2, a length of 1.4 cm, and is fabricated using a 3-mask process. Preliminary experiments show that the primary performance constraint for design A is imposed by the compromise between mechanical robustness and transverse conductance of the thin glass base plate that separates the high pressure and low pressure streams. Design B enhances the robustness of the device and can sustain higher pressure.

I. INTRODUCTION

In cryosurgery, cancerous tumors or other pathological tissues are locally destroyed by repeated freeze/thaw cycles [1]. This procedure is minimally invasive: a narrow cryoprobe is inserted through a small incision and creates a well-controlled cryolesion. The ablated tissue is subsequently absorbed or sloughed by the body. By avoiding excision, operative blood loss and discomfort are minimized.

Recent development of miniature cryoprobes with large refrigeration capacity [2-4] and techniques for real-time monitoring using ultrasound or magnetic resonant imaging [5-7] are allowing cryosurgical techniques to be extended to the treatment of cancers in areas that are not readily accessible [8]. This requires cryoprobes to be miniaturized to a size that permits them to be inserted through a very small incision. This effort examines the possibility of fabricating cryoprobes with micromachining technologies. However, the cooling performance of the cyroprobe must not be compromised: it is known, for example, that temperatures below -50 °C are always necrotic for pathological tissue [9-11]. In addition, a rapid cool-down rate [1, 12] between 25-50 °C/min. and multiple freeze-thaw cycles [13] are preferred to decrease the likelihood of cell survival.

A fully integrated micromachined cryosurgical probe can have significant advantages over the conventional cryosurgical probes in terms of thermal performance, size, flexibility and cost. The Joule-Thomson cooling cycle can meet these requirements with high thermodynamic efficiency [14]. In this cycle (Fig.1), cold, high-pressure fluid leaving a recuperative heat exchanger expands through a valve, resulting in a temperature drop through the valve if the state of the fluid lies below the inversion curve before expansion. Due to the absence of cold moving parts, this cycle can be potentially implemented with reliable structures that are simple enough to be micromachined from silicon and glass.

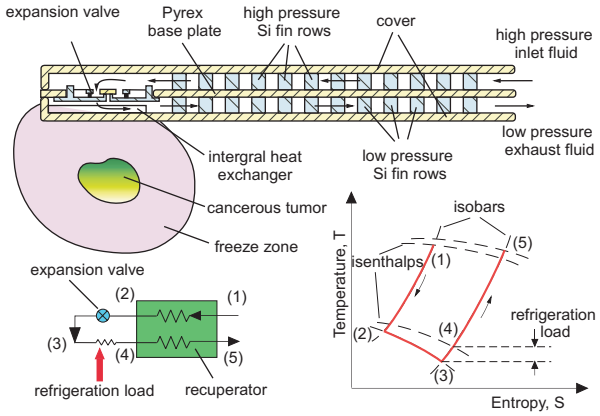

Fig. 1: Joule-Thomson refrigeration cycle. High-pressure fluid obtained from external compressor at state (1) passes through a counter flow recuperative heat exchanger, where it is pre-cooled by the low-pressure fluid returning from the refrigeration load. The cold high-pressure fluid leaving the heat exchanger at state (2) expands through a valve to state (3). The cold, low-pressure fluid is directed through the load heat exchanger where it is warmed by the refrigeration load to state (4) and then is fed back into the heat exchanger.

The recuperative heat exchanger is the most important part of the J-T probe that significantly affects the cooling performance and thermal efficiency. Prior efforts have used a concentric arrangement of commercial glass tubes [15], and flexible polyimide heat exchangers [16], which are not suitable for this application. This paper describes two approaches (planar and stacked) for micromachining recuperative heat exchangers intended for use in J-T cryosurgical probes. Expanding upon our preliminary report on planar devices [17], it includes multi-layered structures that offer different performance compromises and manufacturing challenges.

II. DESIGN & FABRICATION

In J-T cooling cycle, the heat exchanger must maintain good stream-to-stream heat conductance between the high-

* *Corresponding author:* 1301 Beal Ave., Ann Arbor, MI, 48109, USA; Tel: (734) 763-5914, Fax: (734) 763-9324. E-mail: zhuwb@umich.edu

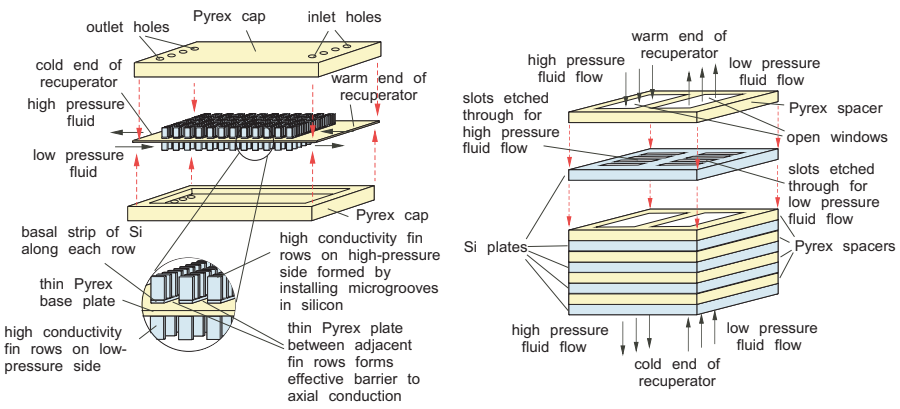

a) Design A: planar heat exchanger. b) Design B: perforated plate heat exchanger.

Fig. 2: Schematic diagram of recuperative heat exchanger design

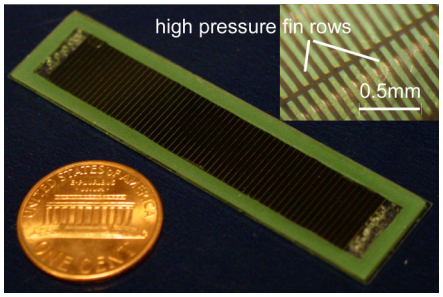

a) The size of planar micro recuperator from design A is 6cm×1.5cm with total 2.5mm thickness. Gap between each fin row is 51μm. Fin size of high pressure fin rows is 50μm×782μm, 200μm high. There is 50μm gap between fins. Fin size of low pressure fin rows is the same as high pressure fins. But the gap between fins is 345μm.

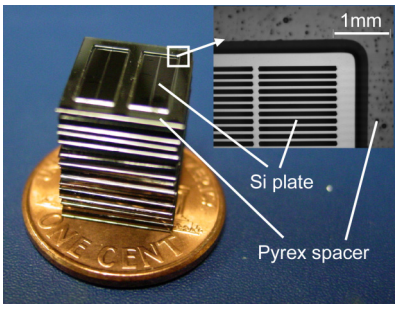

b) The die size of perforated plate micro recuperator from design B is 1×1cm^2. Thickness of Si plate is 500μm. Thickness of Pyrex spacer is 300μm. Two rows of opening slots are on both high pressure and low pressure regions of Si plate. The size of the slot is 50μm wide and 1400μm long; there is 50μm gap between each slot.

Fig. 4: Fabricated heat exchangers

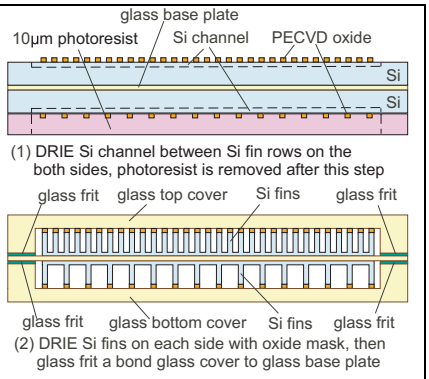

Fig. 3: Fabrication process of planar heat exchanger in design A. Si/glass/Si wafer stack is anodically bonded together. PECVD oxide mask is then coated and patterned on both sides. An oxide layer and a subsequent layer of 10 μm conformal photoresist serve as masks in a two-step DRIE process. This thick resist layer is used to protect the oxide pattern in the first DRIE step. Si channels between each fin row are etched down 20 μm by DRIE before the photoresist is stripped. Si fins is fabricated in the second DRIE step. A glass cap is bonded with glass frit (G1017, from Vitta Corp.) onto the glass base plate after the two-step DRIE process is finished on each side. The glass caps are fabricated from 1.1 mm thick glass wafers. With 500 Å/5000 Å Cr/Au layer as a mask, the wafer is immersed in the HF: HNO_3 solution to create a recess that is 100 μm deep. Inlet and outlet holes are drilled with an electrochemical discharge drilling method.

and low-pressure channels while restricting stream-wise conduction to allow a large enthalpy difference between the two streams and thus achieve high cooling performance. Fortunately, the thermal properties of silicon and Pyrex, respectively, compare favorably with oxygen-free high conductivity (OFHC) copper and stainless steel that are used in conventional heat exchangers. This combination of very high and low thermal conductivity suggests that a silicon and Pyrex composite heat exchanger will be attractive. Two designs (Fig. 2) of Si-glass heat exchanger are developed.

The planar design A (Fig. 2a) uses rows of fins composed of high-conductivity silicon, anodically bonded above and below a thin base plate of low-conductivity Pyrex. The heat transferred from the high pressure fluid into the silicon fin structure is conducted through the thin Pyrex base plate into the low pressure fin structure where the heat is finally transferred into the low pressure fluid. Theoretical models [18，19] show that the Pyrex base plate between the high- and low-pressure channels must be ≤100 μm to maintain adequate refrigeration power. This compromises the structural integrity of the device at elevated pressure difference between two streams.

A five-mask process required two Si wafers and three glass wafers is developed for design A and shown in Fig. 3. A major challenge in this process is to etch the fin structure on each side of the wafer stack by DRIE. The etch must clear the narrow regions between rows, etch between the tightly packed fins, and also clear the perimeter of the device, which has no masked features, and etches faster. A two-step DRIE process, as described in Fig. 3, is used to compensate this DRIE artifact. This etch will ultimately lead to the creation of the basal strip along each row that is illustrated in the magnified part of Fig. 2a in the second DRIE step. This basal strip also adds benefit of strengthening the attachment of the fins to the glass base plate. A similar two-step DRIE process is completed on the other side of wafer stack. Figure 4a shows a fabricated planar heat exchanger.

Design B (Fig. 2b) uses numerous high-conductivity silicon plates alternating with low-conductivity glass spacers. Narrow slots are etched into the Si plate in order to provide two streams with a larger amount of surface area for heat exchanger. Each plate is divided into two regions by glass spacer. The high and low pressure regions are sealed from each other between Si plates and glass spacers. The heat transferred from the high pressure fluid into the silicon plate is conducted through the silicon plate into the low pressure region where it is finally transferred to the low

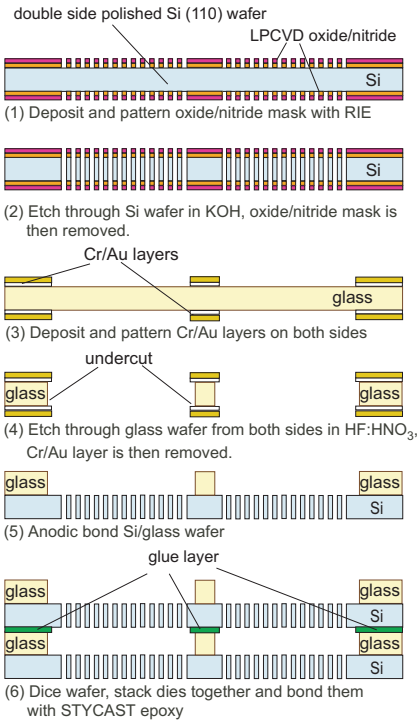

Fig. 5: Fabrication process of heat exchanger in design B.

pressure fluid. The geometries of this design, including number and size of the slots, distance between slots, number of plates, etc., have been numerically optimized [20].

A three-mask fabrication process of design B (Fig. 5) uses KOH wet-etching of (110) Si to obtain vertical sidewalls in the slots on Si plates, and HF:HNO_3 wet etching of glass wafers to fabricate spacers. In order to achieve deep etching in both KOH step and HF:HNO_3 wet etching step, the wafers are patterned and simultaneously etched from both sides until the openings are formed. Figure 6 shows an SEM of the slot structure etched by KOH. The Si wafer and Pyrex wafer is then anodically bonded together. Dies that are diced from the wafer are then stacked together and bonded with STYCAST 2850FT epoxy (Emerson & Cuming) at room temperature. Figure 4b shows a fabricated perforated plate heat exchanger.

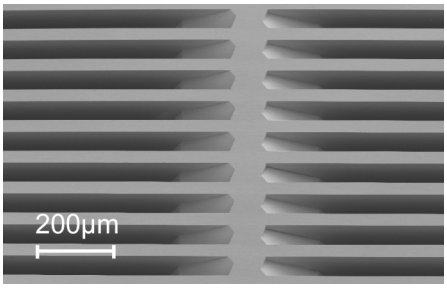

Fig. 6: SEM of slot structure etched by KOH in design B

III. EXPERIMENTAL RESULTS

The planar heat exchanger of design A was installed into a macro-scale self-cooling system (Fig. 7) after leak test. In this experiment, the heat exchanger is placed in a cavity within a piece of Styrofoam insulation and surrounded by fiberglass insulation. The inlet is provided with a flow of butane from a high pressure bottle at room temperature. The pressure, flow rate, and temperature (T_1) of this flow are measured. The high pressure butane passes through the heat exchanger where it is pre-cooled by the low pressure butane returning from the cold end. The butane is expanded through an orifice (a precision jewel installed in a blank gasket) located at the cold end of the system; by varying the size of the orifice, it is possible to control the flow rate through the heat exchanger. The temperatures on either side of the orifice (T_2 and T_3) are measured using thermocouples that penetrate the butane stream.

Figure 8 illustrates the temperature difference between the cold end and the inlet as a function of orifice area for three different inlet pressures. The optimal orifice size is 0.2mm^2. The temperature difference as a function of inlet pressure for this optimal orifice is shown in Fig. 9.

The perforated plate heat exchanger of design B was installed in a similar self-cooling setup and is currently being test at pressures much higher than design A.

IV. DISCUSSION

The self-cooling data of deisgn A was limited to very small temperature differences relative to a practical device that is useful for cryosurgery. This is because the pressure

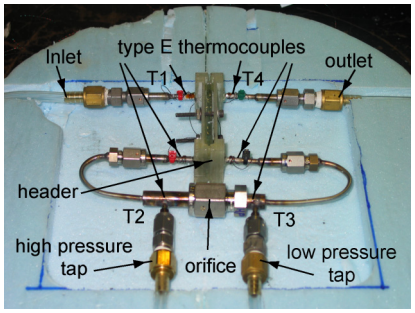

Fig. 7: Self-cooling setup. The micro recuperative heat exchanger is mounted inside the header. The type E thermocouples are inserted into the high and low pressure taps to measure the gas temperature inside the tube.

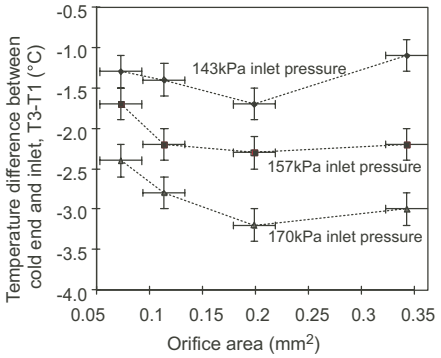

Fig. 8: Design A: the ΔT between inlet and cold end is T_3-T_1, where T_1 is the inlet flow temperature, T_3 is the temperature at the cold end. Cooling performance of the test setup reaches maximum value with orifice size of 0.2 mm^2.

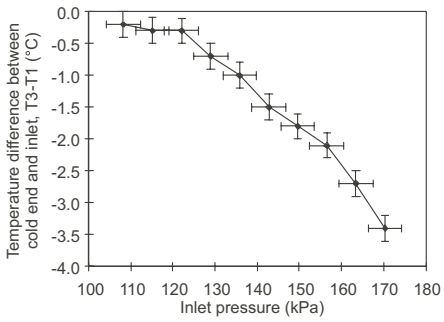

Fig. 9: Design A: Temperature difference between cold end and inlet as a function of the inlet pressure for 0.2 mm^2 orifice area. The measured temperature difference matches the theoretical model assuming a parasitic heat loss of 40 mW.

difference between two streams anticipated for a cryosurgical probe may be as high as 1400 kPa (200 psi) whereas the testing was limited to 70 kPa (10 psi) in order to avoid fracturing the base plate. Theoretically, this thickness of the base plate should be able to sustain larger pressure differences, but in practice this is not true due to fabrication limits. A thicker base plate would provide greater structural integrity, but the increased transverse thermal resistance would further reduce cooling power. In addition, the fin height of 200 μm is much smaller than the initial target of 500 μm. This modification was required by manufacturing constraints, but results in both a 2.5× reduction in heat transfer area as well as a 5× increase in the pressure drop across the heat exchanger.

The predicted and measured effectiveness of design A as a function of mass flow rate (based on the hot side energy balance) is illustrated in Fig. 10. The effectiveness of the heat exchanger (ε) is defined as the ratio of the heat transferred within the heat exchanger to the maximum possible amount of heat that could have been transferred had the heat exchanger been perfect (i.e., the heat transferred if T_4 was equal to T_1). The effectiveness can be computed based on either the hot- or cold-side balance (ε_h or ε_c, respectively):

$$\varepsilon_h = \frac{\dot{q}_{HX,h}}{\dot{q}_{HX,max}} \text{ or } \varepsilon_c = \frac{\dot{q}_{HX,c}}{\dot{q}_{HX,max}},$$

where $\dot{q}_{HX}$ is the actual heat transfer and $\dot{q}_{HX,\max}$ is the ideal heat transfer in perfect conditions. This measured result properly matches the theoretical model.

Preliminary experiments show that the heat exchanger of design B can sustain much higher pressure than design A because the region between two streams is a more than 700μm wide layer with alternating Si and glass. The cooling performance is not sacrificed in this design because the glass layers maintain a high thermal resistance along the flow direction. Simulations [20] show that the predicted cooling performance of design B is close to commercial available cryosurgical probes.

V. SUMMARY

A planar micro heat exchanger of design A with a footprint of 6×1.5 cm^2 and 2.5 mm thickness was fabricated in a 5-mask process using three glass wafers and two Si wafers. In our tests, the self-cooling performance of the micro heat exchanger was mainly limited by (i) mechanical robustness of the glass base plate and (ii) Si fin height that was constrained by the uniformity of DRIE. However, the effectiveness of the heat exchanger varied from 0.8 at a mass flow rate of about 0.01 g/s to 0.6 at 0.075 g/s, which matched the developed theoretical model. A perforated plate design with a footprint of 1×1 cm was then fabricated in a 3-mask process to avoid a fragile base plate when maintaining high thermal resistance along the flow direction. If successful, the robustness, flexibility and performance associated with this new micromachined design may result in the application of cryosurgery to new biomedical areas.

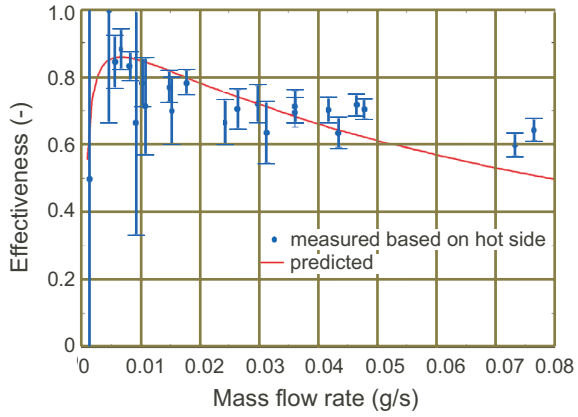

Fig. 10: Design A: measured effectiveness and the predicted effectiveness as a function of the mass flow rate.

ACKNOWLEDGEMENT

This work was funded in part by a grant from the US National Institutes of Health (R33 EB003349-04).

REFERENCES

[1] J. Dobak, "A Review of Cryobiology and Cryosurgery," *Advances in Cryogenic Engineering*, 43, pp. 889-896, 1998

[2] Z. H. Chang, J. J. Finkelstein, J. G. Baust, "Optimization of Cryosurgical Instrumentation for use in Minimally Invasive Prostate Surgery," *ASME Heat Transfer Div Publ HTD*, v 267, pp. 45-55, 1993

[3] B. Z. Maytal, "Fast Joule-Thomson Cryocycling Device for cryosurgical Applications," *Advances in Cryogenic Engineering*, 43, pp. 911-917, 1998

[4] J. Dobak, et al., "A Novel Closed Loop Cryosurgical Device," *Advances in Cryogenic Engineering*, 43, pp. 897-902, 1998

[5] R. Masumoto, K. Oshio, F. A. Jolesz, "Monitoring of Laser and Freezing-Induced of the Liver with Tl-Weighted MR Imaging," *Journal of Magnetic Resonance Imaging*, 2, pp. 555, 1992

[6] B. Rubinsky, et al., "Monitoring Cryosurgery in the Brian and Prostate with Proton NMR," *Cryobiology*, 30, pp. 191-199, 1993.

[7] G.R. Pease, et al., "MR Image-Guided Control of Cryosurgery," *Journal of Magnetic Resonance Imaging*, 5, pp. 753-760, 1995

[8] J. K. Cohen, R. J. Miller, "Thermal Protection of Urethra during Cryosurgery of the Prostate," *Cryobiology*, 31, pp. 313-316, 1994

[9] A. Gage, "Five-year Survival Following Cryosurgery for Oral Cancer," *Archives of Surgery*, 111, pp. 990-994, 1976

[10] A.A. Gage, et al., "Critical Temperature for Skin Necrosis in Experimental Cryosurgery," *Cryobiology*, 19, pp. 273-282, 1982

[11] J. Bischoff, K. Christov, B.A. Rubinsky, "Morphological Study of Cooling Response in Normal and Neoplastic Human Liver Tissue: Cryosurgical Implications," *Cryobiology*, 30, pp. 482-492, 1993

[12] A. A. Gage, et al., "Effect of Varying Freezing and Thawing Rates in Experimental Cryosurgery," *Cryobiology*, 22, pp. 175-182, 1985

[13] A. A. Gage, "Cryosurgery in the Treatment of Cancer," *Surgery, Gynecology & Obstetrics*, 174, pp. 73-92, 1992

[14] E. D. Marquardt, et al., "A cryogenic Catheter for Treating Heart Arrhythmia," *Advances in Cryogenic Engineering*, 43, pp. 903-910, 1998

[15] J. Burger, et al., "169 Kelvin Cryogenic Microcooler Employing a Condenser, Evaporator, Flow Restriction and Counterflow Heat Exchangers" *Proc. IEEE MEMS*, pp. 418-421, 2001

[16] J.C. Selby, M.L. Philpott, M.A. Shannon, "Fabrication of Mesoscopic, Flexible, High Pressure, Microchannel Heat Exchangers (MHEx)," *Trans of NAMRI/SME*, Vol. 29, pp. 469-476, 2001

[17] W. Zhu, D.W. Hoch, G.F. Nellis, S.A. Klein, Y.B. Gianchandani, "A Planar Glass/Si Micromachining Process for the Heat Exchanger in a J-T Cryosurgical Probe," *Proc. Solid State Sensors, Actuators and Microsystems Workshop*, Hilton Head, pp.51-55, 2006.

[18] G.F. Nellis, "A Heat Exchanger Model that Includes Axial Conduction, Parasitic Heat Load, and Property Variations," *Cryogenics*, 43(9), pp. 523-38,'03.

[19] M. Frank, M, *Recuperative Heat Exchanger for a MEMS Cryoprobe*, M.S. Thesis, Univ. Wisconsin, Dept. of Mechanical Engineering, 2004

[20] D. W. Hoch, et al., "Progress Towards a Micromachined Heat Exchanger for a Cryosurgical Probe," *Proc. the 14th International Cryocoolers Conference*, Annapolis, Maryland, 2006.